Chapter 12

Mathematical Modeling of Cell Adhesion and Its Applications to Developmental Biology and Cancer Invasion

Alf Gerisch[1] and Kevin J. Painter[2]

Contents

12.1 Introduction

From the earliest embryonic stages through to the complexity of the adult, the ability of cell populations to adhere to either each other or the surrounding extracellular matrix (ECM) is of critical importance to the survival of the organism. During embryonic

[1]A.G. gratefully acknowledges financial support by the Division of Mathematics, University of Dundee during a long-term visit in 2007 introducing him to the topic.

[2]K.J.P. is supported in part by the Integrative Cancer Biology Program Grant CA113004 from the U.S. National Institutes of Health, by a BBSRC grant BB/D019621/1 to the Centre for Systems Biology at Edinburgh, and by the Mathematical Biosciences Institute, Ohio State University, Columbus, Ohio.

development, carefully regulated adhesion plays a fundamental role directing the various cell populations into the developing organs while maintaining strong adhesive contacts is essential in preserving the integrity and structure of the adult tissues. The manifest importance of cellular adhesion is exposed due to its abnormal functioning in a wide variety of pathological conditions, including malignant cancer growth (e.g., [49]) and cardiovascular diseases (e.g., [40]).

Adhesion can generally be classified into two principal forms: *cell-cell adhesion* and *cell-matrix adhesion*. The former defines the direct binding between cells through the creation of transmembrane protein-protein complexes, the prototype example of which are the strong contacts maintaining epithelial structures such as the epidermal skin layer. The latter describes the attachment of cells to the surrounding ECM, the scaffold support surrounding cells and composed of a variety of molecules including collagens, fibronectins, and laminins. While the ECM is present in all tissues, its prevalence in connective tissues such as the dermal skin layer makes cell-matrix adhesion particularly important for stromal populations such as fibroblasts and immune cells.

The control of cell-cell and cell-matrix adhesion is fundamentally determined through the expression and regulation of a wide variety of membrane-based proteins, the cell adhesion molecules (CAMs); for a general review, see [1]. Four principle families of CAMs have been classified: the cadherins (e.g., E-cadherin, N-cadherin); the immunoglobin superfamily (e.g., NCAM, EpCAM); the integrins; and the selectins. Members of these families generally consist of transmembrane molecules with an intracellular domain linking to intracellular signaling pathways and an extracellular domain connecting to other cells or the matrix. Adhesion is achieved through protein-protein coupling of the extracellular domain to form either *homophilic* interactions (i.e., binding between two proteins of the same type, such as E-cadherin–E-cadherin) or *heterophilic* interactions (binding between two molecules of different type).

The cadherins form a large family of transmembrane adhesion molecules widely recognized for their capacity to mediate direct cell-cell adhesion, although their function extends to a host of other cellular processes, ranging from apoptosis to signaling (for reviews on the behavior and function of cadherins, see [36,57]). Classic cadherins tend to form homophilic interactions in the intermembrane space separating two cells, although heterophilic interactions can also occur (e.g., E-cadherin–P-cadherin), albeit with different adhesive intensity [25]. The transmembrane binding fastens cells in a zipper-like manner, conferring a key role to cadherins in all aspects of an organism's lifespan, from coordinating multicellular tissue movements during development to maintaining the tissue structure of the adult. A wide variety of cadherins have been identified, distributed across different cell populations. For example, the E-cadherins are mainly associated with epithelial cell populations, while more migratory, mesenchymal cells (e.g., fibroblasts) tend to favor N-cadherins [79].

The integrins form the dominant CAMs regulating adhesion to the extracellular matrix [10]. The extracellular domain couples the cells to ligands of the ECM to create various types of cell-matrix adhesion structures that, in turn, modulate the intracellular component to interact with intracellular signaling. These adhesion structures have the capacity to recruit additional molecules (e.g., matrix proteases) and

therefore locally alter the structure of the ECM. Dynamic control cell-matrix adhesion is crucial to the migration of cells in ECM-rich environments, such as connective tissue, where migration proceeds through a continuous cycle of attachment at the leading edge, extension and translocation of the cell body, and detachment at the cell rear (e.g., see Friedl and Wolf [29]). Consequently, the structure of the ECM plays a significant role in directing migration: certain cells may migrate toward ligand-dense (i.e., more adhesive) regions of the matrix, a process termed *haptotaxis*; toward more rigid regions, called *durotaxis* [46]; or even along the aligned collagen fibers, called *contact guidance* [26].

12.1.1 Cell Adhesion during Pattern Formation and Development

In a series of classical experiments, Townes and Holtfreter [74] demonstrated the intrinsic capacity for certain embryonic cell populations, when dissociated and randomly mixed, to spontaneously reorganize into their original embryonic relationship, a process attributed at the time to "tissue-affinity." The underlying mechanism(s) governing this "cell-sorting" have been the subject to a significant degree of speculation and experimentation over the years, with the Differential Adhesion Hypothesis (DAH) of Steinberg (see the reviews [27,68] of Foty and Steinberg) to the fore of theories. The series of experiments by Steinberg in the 1960s [65–67] demonstrated that embryonic cell types obey strict rules: Whatever the initial distribution for two separate populations was, the cells always rearranged into the same configuration, Figure 12.1a. Furthermore, populations formed hierarchical relationships: If cells of type B are engulfed by cells of type A and cells of type C are engulfed by cells of type B, then C will always be engulfed by A; see Figure 12.1b.

Based on these observations, the DAH employs thermodynamic principles, proposing that cell sorting derives from variation in cell surface tensions that, in turn, depend on the different adhesive properties between the cell types; Cells are assumed to rearrange in a manner to minimize their free adhesive energy, analogous to the behavior of two immiscible liquids. Through these arguments, a mixture of two cell populations, A and B, can be predicted to rearrange into four basic configurations according to the relative strengths of self-adhesion (i.e., the binding between two cells of the same type, S_{AA} and S_{BB}) and cross-adhesion (i.e., binding between two cells of different type, C_{AB}): mixing, engulfment, partial engulfment, and complete sorting; see Figure 12.1c.

Over the past decade or so, a series of thorough experiments have substantiated the DAH for sorting (see reviews [27,68] for further details). Experiments with two cell lines expressing different levels of cadherins (and hence varying degrees of adhesiveness) resulted in the population expressing higher cadherin levels aggregating to the center, with the other line confined to the periphery, consistent with the predictions of the DAH [25,69]. Recent experiments of Foty and Steinberg, [28] have directly linked the surface tensions underlying sorting of tissues to differing strengths of cell-cell adhesion.

The capacity for differential adhesion to spatially sort out different populations implies an important role during the morphogenetic patterning of the embryo; indeed,

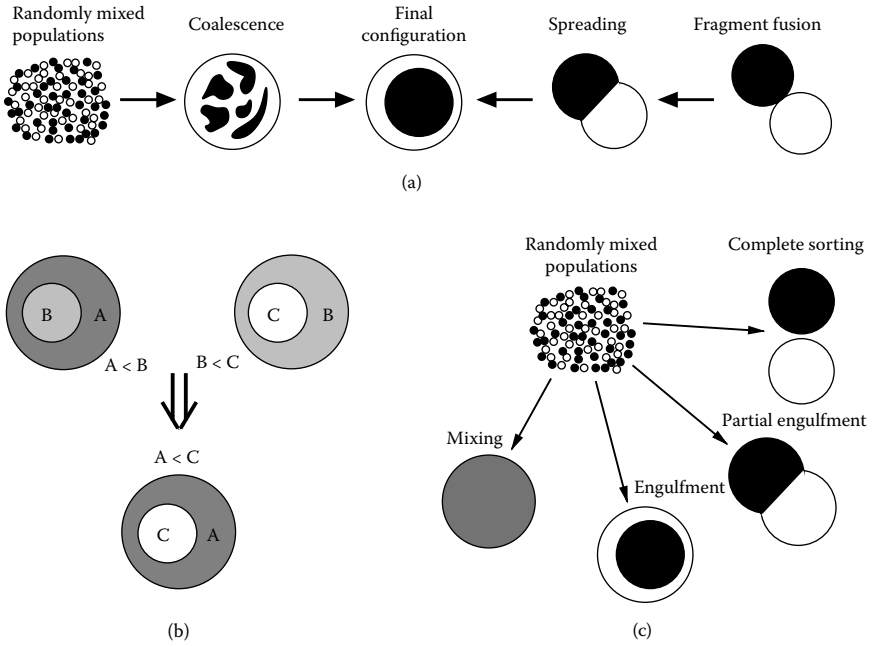

Figure 12.1 Sketches showing the behavior of two adhesive cell populations, as predicted by the DAH. (a) The same populations always approach the same final configuration, regardless of initial distribution. Starting from the left, populations of mixed and dissociated cells coalesce before evolving to a final configuration (shown here as "engulfment"). Starting from the right, the same two populations, when placed together as fragments, spread over one another before reaching the same pattern. (b) Hierarchical relationships in adhesive populations. (c) Two populations, A and B, evolve into various final configurations according to their self-adhesion S_{AA}, S_{BB} (between A and A, between B and B) and cross-adhesion C_{AB} (between A and B) strengths. For two populations, the observed patterns are *mixing* (in which the populations are uniformly distributed–requires dominant cross-adhesion $C_{AB} > \frac{S_{AA}+S_{BB}}{2}$), *engulfment* (in which the more cohesive population is engulfed by the less cohesive population–requires $S_{BB} < C_{AB} < S_{AA}$ or $S_{AA} < C_{AB} < S_{BB}$); *partial engulfment* (for which the cross-adhesion strength is less than both the self-adhesion strengths–$C_{AB} < S_{AA}$ and $C_{AB} < S_{BB}$); and *complete sorting* (for which $C_{AB} = 0$ and the two populations form separate aggregations). (Figures adapted from [27].)

examples of spatio-temporally controlled alterations to the adhesive properties of cells and the matrix include whole-embryo tissue movements during gastrulation, formation of the boundaries during segmentation of the hindbrain, and the precisely controlled movements of differentiated cell types during the patterning of the insect compound eye (for these and further examples, see [13,36,44,68,72,73]). In segmentation, the embryo is subdivided into a number of discrete blocks along the

anterior–posterior axis, laying a blueprint for future development. For a number of organisms, including birds, fish, and mammals, this proceeds through *somitogenesis*, in which parallel stripes of mesenchymal tissue (the paraxial mesoderm) metamerically pinch off to form somitic pairs on either side of the developing neural tube. Compaction from the mesenchyme into epithelialised somites is thought to arise through increases to cell adhesion [16], with a number of studies indicating roles for both matrix molecules such as fibronectin (e.g., [24,53]) and cadherins (e.g., [45,71]). Somites undergo subdivision, first into distinct anterior and posterior portions (e.g., [59]) before they subsequently sort into further embryonic subpopulations [8]. Differential cell-cell adhesion has been suggested to pattern somites into their anterior and posterior segments [70], a theory strengthened by the distribution of various cadherins in the developing somite (e.g., [24,42]).

12.1.2 Cell Adhesion in Cancer Invasion

Understanding the processes that regulate the control of adhesion during tissue development and homeostasis is crucial when it comes to determining the factors that lead to tumor progression. The transition from a benign, compact tumor to an invasive, spreading tumor capable of forming metastases is a pivotal moment for prognosis, and it is now widely accepted that modifications to the adhesive properties of the cells and surrounding ECM correlate with malignant development for a wide range of different cancer types (e.g., [14,15,17,49]).

For many tumors of epithelial origin, a link between increased malignancy and progressive loss of function in the cell-cell adhesion molecule E-cadherin has been observed [17], with forced expression of E-cadherin in cultures resulting in a reversal from an invasive to benign phenotype (e.g., [11]). In a number of cancers, the loss of E-cadherin is accompanied by a gain in N-cadherin expression, a "cadherin-switching" mechanism [79] similar to those seen in various embryonic processes—for example, ingression of cells through the primitive streak. Such transitions are believed to give rise to the evolution of a more invasive/migratory form.

To infiltrate surrounding healthy tissue it is necessary for the tumor cells to interact with the surrounding ECM, a structure that can both provide a substrate through which cells can move as well as a physical barrier against migration. To migrate, cells must attach to the matrix through the formation of focal adhesions, mediated through the integrin family of CAMs. These focal adhesions provide a site for recruiting matrix proteases (e.g., MMPs) that degrade the ECM and hence provide space for tumor invasion and expansion to occur [29]. A wide number of *in vitro* and *in vivo* studies have investigated the importance of integrins and MMPs for cancer cell invasion, yet the precise impact on invasion (e.g., promoting or inhibiting) varies widely according to cancer origin.

The form of the invasive front is also variable, with different tumors displaying diverse patterns of invasion, often resulting in an indistinct and diffuse tumor/host tissue interface [29]. Certain tumors (e.g., lymphomas, glioblastomas) tend to invade as individual cells, occasionally forming single-file cell chains known as "indian-chains" (e.g., in breast carcinomas). Other tumor types, particularly those of epithelial

origin, tend to invade in a collective fashion in which multicellular strands of tumor cells known as "fingers" protrude into the host tissue or cell clusters migrate out from the tumor while maintaining close contacts. Once again, these distinct patterns of invasion correspond to different patterns of CAM expression, with the individual-cell migration phenotypes, typified by mesenchymal/amoeboid cell types, expressing high levels of integrins and proteases while collective-cell invasion is characterized by epithelial cell types with strong cell-cell adhesion.

12.1.3 Chapter Outline

Clearly, cellular adhesion plays a crucial role in many biological processes. While a wide range of models have incorporated adhesion at the discrete level, the incorporation into continuous models has received relatively little attention, a fact that can be attributed primarily to a lack of models able to replicate the characteristic behaviors of adhesive populations. In this chapter we first explore the history of modeling in this fundamental process. We proceed to review the derivation of the continuous model for cell-cell adhesion developed in [6] and show how it captures the fundamental properties of aggregation and cell-sorting. In Section 12.5 we consider an application of this model to tumor invasion [33,64]. Finally, we raise a number of biological, modeling, analytical, and numerical challenges stimulated by these works.

Supplementary material for this chapter, including color figures and simulation movies, is available online at

`http://sim.mathematik.uni-halle.de/gerisch/2009/GerischPainter09/`

12.2 Mathematical Modeling of Cell Adhesion

The recognition of cellular adhesion as a major driving force behind various biological processes has led to the development of a variety of modeling approaches and models. Naturally, the structure of a model will inevitably depend on the precise biological question to be addressed. However, it is reasonable to expect that for any model of cell-cell adhesion, at a *population* level it should capture core properties, such as an ability to predict the aggregation/coalescence of a population as the "adhesivity" of the cells is increased and, when expanded to include multiple populations, the various sorting properties predicted by the DAH. The mechanism of cell-cell adhesion—a nonlocal interaction between two cells through transmembrane receptor binding—naturally suggests the usage of discrete cell (i.e., individual cell or agent-based) approaches, which retain the finite cell size and permit relatively straightforward incorporation of the molecular interactions and/or forces that act between the cells. Weighed against such advantages, however, are the significant computational times required to simulate large populations and difficulties in obtaining analytical insight. Consequently, it is

desirable to augment such methodologies with continuous models that capture the dynamics of population-level behavior.

12.2.1 Discrete Models for Cell Adhesion

The past decade has witnessed the development of a wide variety of discrete models that incorporate cell adhesion and are of increasing sophistication. Generally, such models can be classified into two major classes: lattice-based and lattice-free approaches. We start this section with a brief discussion of a number of discrete lattice-based models (the book by Deutsch and Dormann [21] reviews these models in greater detail with a specific focus on cellular adhesion in its Chapter 7) and consider cellular automata, the discrete-continuum technique, and Cellular Potts models.

In lattice-based approaches, the morphology of a cell is restricted according to some underlying discretization of space, which can be either regular (e.g., rectangular or hexagonal in two dimensions) or irregular (e.g., a voronoi tessellation). These approaches can generally be further subclassified into those for which one cell correlates to one lattice site and spatially extended approaches, with a cell defined by a connected set of sites. Examples of the former class include many cellular automata models: for the evolution of cells under the influence of differential adhesion, see, for example [20]; in [50], a similar approach was employed to demonstrate how different adhesive properties can generate zebrafish pigmentation stripes. A second example of the single-site class is the discrete-continuum technique developed by Anderson and co-workers [2,4]. Here, the discrete cells interact with each other and surrounding continuous fields representing extracellular matrix densities and growth factor concentrations. Movement probabilities are derived from these interactions, which include adhesion of cells to the extracellular matrix, and drive the reorganization of the cell pattern in space and time. The primary application of this technique has been in models of tumor cell invasion.

A prime example of a spatially extended approach is the Cellular Potts Model (or Glazier-Graner-Hogeweg model). Originating in theoretical physics, it was adapted and applied to cell populations by Graner and colleagues in the 1990s (see [34,35]). Here, each (biological) cell is of a certain cell type and represented as a number of sites (vertices) of a regular lattice. For a given state of the system, a Hamiltonian function is defined based on the surface energy along the cell boundaries and deviations of cell sizes from typical values. The evolution of the system is then driven by a Monte-Carlo-like scheme that aims to reduce the value of the Hamiltonian by changing the cell association of a randomly chosen lattice site to that of one of its neighboring sites. The surface energy depends on the cell types on either side of the cell surface and consequently accounts for self- and cross-adhesive effects. A background medium (e.g., representing the extracellular matrix) can also be included in the model. The generic model structure of this Potts model has been elaborated by various authors to make it suitable for particular application areas, for example, cellular slime mold morphogenesis [48], vertebrate development [58], epidermal homeostasis [62], solid tumor growth [75], and angiogenesis [9].

The artificiality of the imposed grid can be countered through the adoption of a lattice-free approach in which individual cells are allowed to move freely through continuous space. In a number of models of this type, cells are given variable, yet predefined, shapes such as deformable ellipsoids of fixed volume in a model for cell movement of *Dictyostelium discoideum* [19,55,56]. Another option, which allows for cell growth and division, is that the *average* cell shape at any point in the life cycle of a cell is predefined while the *actual* cell shapes are reconstructed from that by taking neighboring cells into account. This approach, introduced by Drasdo et al. [23], is followed in models of tumor growth, epidermal homeostasis, and early development; for a brief review and further references, we refer the reader to [30]. One recent extension of this approach has been the incorporation of intracellular and transmembrane molecular interactions, courtesy of an ordinary differential equation system for each cell that describes the regulation of E-cadherin through the β-catenin signaling pathway [60]. In both these and the deformable ellipsoid model described above, movement of individual cells is driven by equilibrating forces, including adhesive ones; alternatively, as in [23], movement is governed by a Monte-Carlo algorithm based on a suitable interaction potential.

A number of further lattice-free models provide even greater flexibility to the manner in which cells refine their shape. The model of Schaller and Meyer-Hermann [63] adopts a Voronoi-Delaunay method, permitting cells to shift between smoothly spherical and polyhedral with increasing tissue density, thereby providing greater control over the amount of cell-cell contact. The subcellular element model of Newman [51] provides additional intracellular structure through subdividing each cell into a set of continuously deforming elements, giving high malleability to the shape of a cell according to its interactions with neighbors and the environment. Finally, in the immersed boundary models for individual cells [22,61], each cell is described as a fluid-elastic structure in which its membrane is represented by a deformable boundary immersed in a fluid. Force balances again are used to represent the adhesive forces that describe the movement and deformation of cells while channels at the membrane permit the influx of fluid into the cell required for growth.

12.2.2 Continuous Models Incorporating Cellular Adhesion

While discrete models for cells permit the straightforward incorporation of many intra-, extra-, and intercellular processes, they also have their drawbacks. Of particular concern is that the transition from the cellular to the tissue scale can require a formidable number of cells, which in many models—and certainly for the more detailed ones—is computationally infeasible. In addition, discrete models often resist a thorough analytical investigation that can shed light on generic properties of the system under study. Both of these issues can be relaxed by considering continuum-scale (PDE) models where cells are represented through their density at the tissue level, and events at the cellular level are accounted for by the particular choice of terms and parameter functions in those models. In the following we briefly review some continuous models that account for cellular adhesion.

The modeling of cell-extracellular matrix adhesion has been phenomenologically captured in a number of models through the idea of "haptotactic" migration (e.g., [3]). Here, cells are assumed to migrate up gradients in the density of an extracellular matrix through the incorporation of an advective-flux type term qualitatively the same as those traditionally employed in continuous chemotaxis models (e.g., [39]).

Incorporation of cell-cell adhesion, however, has proved generally problematic at a continuous level. One approach, adopted in a number of models (e.g., [41]) has been to include cell-cell adhesion through a density-dependent cell diffusion coefficient. While this phenomenologically captures one aspect of adhesion (i.e., the restricted movement of cells in regions of high density), its capacity to describe more complex phenomena such as self-aggregation and sorting of multiple populations is unknown. Byrne and Chaplain [12] presented a model of cancer growth and invasion that accounts for cell-cell adhesion through the incorporation of a surface tension force at the tumor surface controlling the evolution of the tumor shape during growth. This idea has been taken up and extended in recent models [18,47]. The single-phase approach in these models has been broadened to multiphase using a diffuse interface framework in [80]. This model accounts for cell-cell and cell-matrix adhesive effects by incorporating them into a system energy that drives the system following an energy variation scheme. The nonlocal energy term is assumed to be sufficiently localized and the corresponding truncated expansion of that term leads to a fourth-order PDE model of Cahn-Hilliard type.

The modeling approach of Armstrong et al. [6], which is the focus of this chapter, also employs nonlocal terms to account for adhesive effects. In contrast to [80], no expansion of these terms is performed so that the resulting model equations are nonlocal or integro PDEs of second order. This approach has been employed to show that upregulated adhesion can drive both the formation and subsequent anterior-posterior compartmentalization of somites [7] and, as we expand on below, incorporated into models for tumor invasion [33,64].

A highly desirable objective is to develop continuous models for cellular adhesion as the appropriate limit from an underlying individual model for cell movement; in the case of chemotactic cell movement; this has been studied in detail (see [37] for a review) and an obvious advantage lies in the determination of the macroscopic parameters (such as diffusion coefficients and chemotactic sensitivities) in terms of measurable microscopic parameters (e.g., cell velocities, turning rates). A number of recent attempts have been made to approach this problem. In [77], a 1-D representation of a Cellular Potts Model incorporating adhesion was taken, under specific scaling arguments, to its continuous limit, yet the resulting model is relatively unwieldy and it has not been shown whether sorting properties can be captured. Another approach adopted is to consider the evolution of a particle executing one-step jumps on a discrete lattice (e.g., [5,54]). While these models can capture self-aggregation of a population, the ill-posed nature of the resultant continuum equations can create singular behavior. Finally, [52] considers the limit of a Langevin-based individual model. Interestingly, the resulting continuum model incorporates nonlocal terms similar to those of the phenomenological model of Armstrong et al. [6], described below.

12.3 Derivation of a Nonlocal Model for Cell Adhesion

We begin by reviewing and extending the phenomenological derivation for an integro-partial differential equation model for cell-cell adhesion first developed in [6]. Here, a mass conservation approach was employed in which the cell density for an adhesive cell population $u(\mathbf{x}, t)$ ($\mathbf{x} \in \mathbb{R}^n$) was proposed to be governed by:

$$\frac{\partial u(\mathbf{x}, t)}{\partial t} = -\nabla \cdot \mathbf{J} + h(\cdot) \tag{12.1}$$

where $\mathbf{J}$ represents the cell flux and $h(\cdot)$ describes cell kinetics. A multitude of factors are known to dictate cell movement *in vivo*, ranging from long-range chemoattractants to local cell-cell and cell-ECM interactions, indicating a flux of the form

$$\mathbf{J} = \mathbf{J}_{\text{random}} + \mathbf{J}_{\text{adhesion}} + \mathbf{J}_{\text{taxis}} \tag{12.2}$$

where $\mathbf{J}_{\text{random}}$ is the flux due to "random cell movement" (typically modeled as a Fickian diffusion, $\mathbf{J}_{\text{random}} = -D_u \nabla u$, where D_u is the cell diffusion coefficient), $\mathbf{J}_{\text{adhesion}}$ is the flux due to adhesion, and $\mathbf{J}_{\text{taxis}}$ is the flux due to long-range substances such as chemoattractants. For the latter, the classical assumption is to take $\mathbf{J}_{\text{taxis}} = u\chi(u, c)\nabla c$, where c represents the chemoattractant concentration and the function χ is referred to as the chemotactic sensitivity [39,43].

To model the contribution of adhesion to the cell flux, $\mathbf{J}_{\text{adhesion}}$, we assume that movement occurs due to the forces generated when cells bind with other cells or the surrounding matrix, the density of which we denote by $m(\mathbf{x}, t)$. For a cell at $\mathbf{x}$, binding with a cell at $\mathbf{x}+\mathbf{r}$ will create a *local force* $\mathbf{f}$ in the direction $\mathbf{r}$ (equally, the cell at $\mathbf{x} + \mathbf{r}$ experiences the opposite force). To describe adhesion-based movement, we assume that the size of this local force depends on the "adhesivity" of this site, namely the numbers and types of adhesion molecules. Rather than explicitly modeling the concentrations of such molecules, the adhesivity is taken to simply depend on the cell density (indicating the likelihood of forming a cell-cell bond) and the matrix density (indicating the likelihood of forming a cell-matrix bond) at $\mathbf{x} + \mathbf{r}$ through the function $g(u(\mathbf{x} + \mathbf{r}, t), m(\mathbf{x} + \mathbf{r}, t))$. Note that the density of additional cell types can be included here, allowing for cross-adhesion between cell types. The possibility of a cell at $\mathbf{x}$ forming a bond at $\mathbf{x}+\mathbf{r}$ is further expected to depend on the distance between the two sites: cells establish adhesive bonds at the membrane-substrate interface, yet their capacity to change shape (e.g., become elongated) or extend thin cell protrusions ranging from shorter range lamellipodia to longer range filopodia (occasionally up to 100 μm in length, [81]) suggests that the probability of forming bonds may vary with distance.

Together, these assumptions lead us to propose the local force generated at $\mathbf{x}$ via adhesive binding at $\mathbf{x} + \mathbf{r}$ to be

$$\mathbf{f}(\mathbf{x}, \mathbf{r}) = \frac{\mathbf{r}}{|\mathbf{r}|}\Omega(|\mathbf{r}|)g(u(\mathbf{x} + \mathbf{r}, t), m(\mathbf{x} + \mathbf{r}, t)) \tag{12.3}$$

where the right-hand-side terms break down into the direction of the force (a vector), the dependence of the force magnitude on the distance at which bonds are formed, Ω (a scalar), and the dependence of the force on the adhesivity, g (a scalar). We discuss various functional forms for these terms below.

The *total* force exerted at $\mathbf{x}$, $\mathbf{F}(\mathbf{x})$, will be the sum of all local forces $\mathbf{f}(\mathbf{x}, \mathbf{r})$, where $\mathbf{r}$ ranges over a finite volume V indicating the "sensing region": the space over which the cell at $\mathbf{x}$ can make adhesion bonds. As described above, this V is minimally determined by the mean cell volume, yet is likely to be significantly larger due to cell shape change and protrusions. Thus, we compute the total force to be

$$\mathbf{F}(\mathbf{x}) = \int_{\mathrm{V}} \frac{\mathbf{r}}{|\mathbf{r}|} \Omega(|\mathbf{r}|) \mathrm{g}(\mathrm{u}(\mathbf{x}+\mathbf{r}, \mathrm{t}), \mathrm{m}(\mathbf{x}+\mathbf{r}, \mathrm{t}))\, \mathrm{d}\mathbf{r} \tag{12.4}$$

To incorporate the above into the mass balance Equation (12.1), we note that at the low speeds of eukaryotic cell migration (typically 0.1 to 10 μm/min, according to cell type) we can reasonably expect inertia to be negligible and drag proportional to velocity and the cell radius R (Stokes law for a ball of radius R in a laminar flow). The adhesive flux will then be proportional to the cell density and the forces between them and therefore we take

$$\mathbf{J}_{\text{adhesion}} = \frac{\phi \mathrm{u}}{R} \mathbf{F} \tag{12.5}$$

where ϕ is a constant of proportionality. Finally, we substitute Equation (12.5) with $\mathbf{F}$ as given in Equation (12.4) into Equation (12.2), and assume Fickian diffusion and a generic taxis cue $\mathrm{c}(\mathbf{x}, \mathrm{t})$ to obtain the following cell density evolution equation:

$$\frac{\partial \mathrm{u}(\mathbf{x}, \mathrm{t})}{\partial \mathrm{t}} = \overbrace{\mathrm{D_u} \nabla^2 \mathrm{u}}^{\text{Random movement}} - \overbrace{\nabla \cdot (\mathrm{u} \chi(\mathrm{u}, \mathrm{c}) \nabla \mathrm{c})}^{\text{Taxis movement}} - \overbrace{\nabla \cdot \left[\frac{\phi \mathrm{u}}{\mathrm{R}} \int_{\mathrm{V}} \frac{\mathbf{r}}{|\mathbf{r}|} \Omega(|\mathbf{r}|) \mathrm{g}(\mathrm{u}(\mathbf{x}+\mathbf{r}, \mathrm{t}), \mathrm{m}(\mathbf{x}+\mathbf{r}, \mathrm{t}))\, \mathrm{d}\mathbf{r} \right]}^{\text{Adhesive movement}} + \overbrace{\mathrm{h}(\cdot)}^{\text{Cell kinetics}} \tag{12.6}$$

The above forms our basic model for cell adhesion and, when combined with appropriate dynamics for matrix and chemical signaling, can be applied to a wide range of biological processes; a version of the above equation was first considered in [6] to model the basic properties of an adhesive population and, through the incorporation of an extra adhesive population, extended to model cell sorting (see Section 12.4). An amalgamation of Equation (12.6) into a chemical signaling system has been developed to model somite formation during embryonic development (see [7]); and the incorporation into the modeling of tumor invasion has been considered in [33] and [64] (see Section 12.5).

12.3.1 Cohesion through Adhesion

A fundamental test for any model for cell-cell adhesion is to determine its capacity to predict the organization of a population of dispersed cells into aggregations:

Populations of cell lines aggregate rapidly into large and cohesive clumps with increasing cadherin expression (e.g., [28]). To demonstrate the ability of Equation (12.6) to allow this basic phenomenon, we neglect any effects from cell-matrix adhesion and chemoattractants and ignore cell kinetics (i.e., cell growth is assumed to be negligible on the time scale of adhesion-driven movement) to derive:

$$\frac{\partial u(\mathbf{x}, t)}{\partial t} = D_u \nabla^2 u - \nabla \cdot \left[\frac{\phi u}{R} \int_V \frac{\mathbf{r}}{|\mathbf{r}|} \Omega(|\mathbf{r}|) g(u(\mathbf{x} + \mathbf{r}, t))\, d\mathbf{r} \right] \tag{12.7}$$

It remains to define appropriate functional forms for the various components in the nonlocal term. In the simulations that follow, we restrict to two spatial dimensions and therefore take the cell sensing region V to be the circle of radius R. The function Ω defines the dependence on the distance from $\mathbf{x}$. The simplest assumption is to assume that Ω is constant throughout the sensing region; however, a form in which Ω decreases due to the diminished likelihood of forming a bond with distance from the cell may be more appropriate. For the purposes here, we adopt the simplest form and take $\Omega(|\mathbf{r}|) = \text{constant}$; the impact of other forms has been considered in [64] for a 1-D version of the model.

For the adhesivity component, with *attractive* interactions we expect g to (at least initially) increase with cell density u due to the increased likelihood of forming bonds within areas of higher cell densities (and hence more adhesion receptors). Yet at even higher cell densities, it is reasonable to expect the attractive force magnitude to either saturate (e.g., due to all receptors becoming bound) or even decrease (due to an impedance against migrating into "crowded" regions). To explore the impact from different forms of g, we consider respectively a "linear," a "saturating," and a "logistic" form, all depending on an adhesion parameter α:

$$g(u) = \alpha u, \quad g(u) = \frac{\alpha u}{K + u}, \quad g(u) = \alpha u \max\left\{0, 1 - \frac{u}{U_{max}}\right\} \tag{12.8}$$

We have solved Equation (12.7) for each functional form of g from Equations (12.8) on a square spatial domain $(0, 10)^2 \subset \mathbb{R}^2$ with periodic boundary conditions. The initial cell density $u(\mathbf{x}, 0) = 0.1 + \mathcal{U}(\mathbf{x})$ is constant with a uniformly distributed perturbation $\mathcal{U}(\mathbf{x}) \in 10^{-2}[-0.5, 0.5]$. The sensing region V is a circle of radius one and the other parameters used are

$$D_u = \phi = R = 1\,, \quad \Omega(|\mathbf{r}|) = 1 \quad \text{for } |\mathbf{r}| \in [0, 1]\,, \quad \alpha = 30\,, \quad K = U_{max} = 2 \tag{12.9}$$

The numerically computed cell density $u(\mathbf{x}, t)$ at three output times t is shown in Figure 12.2. With the setting described above, we observe aggregation of cells for all three functional forms of g given in Equations (12.8). With the linear form of g, we obtain a very fast aggregation process leading to many small cell clusters with large cell density in the region of up to 20. As time proceeds, some of these clusters coalesce, leading to a further increase in cell density; see Figure 12.3 (left). The diffusion in the model prevents a further increase (also the finite grid width contributes to this; on finer

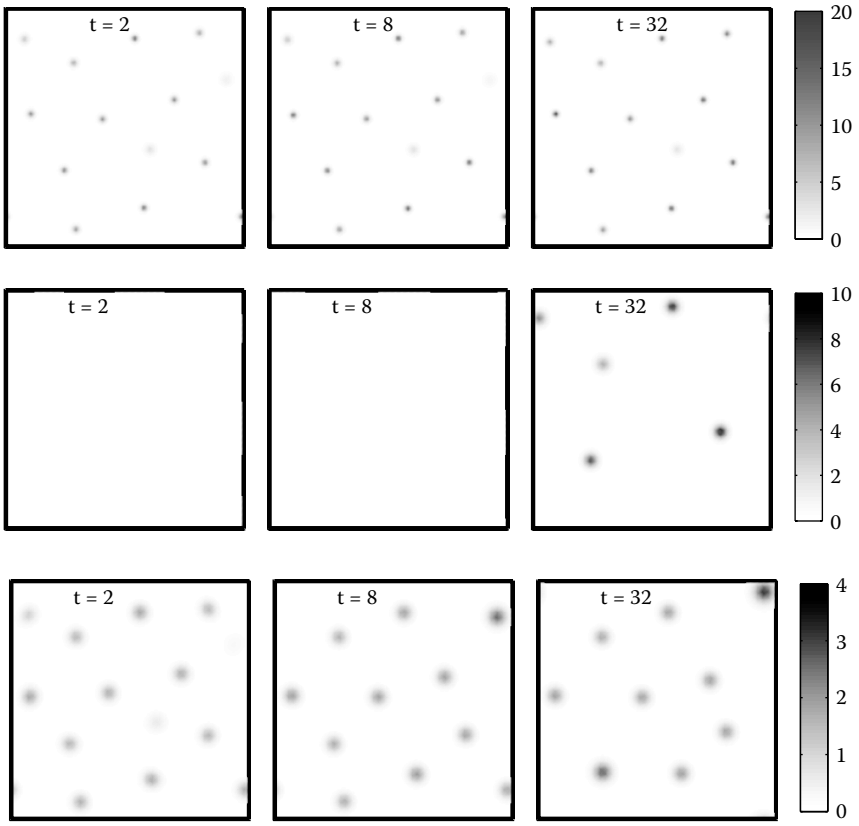

Figure 12.2 Simulation results u(**x**, t) for Equation (12.7) with linear (top row), saturating (middle row), and logistic (bottom row) form of function g; see Equations (12.8), at three output time points t. Note the different color scalings for the three functional forms of g; values of u below 0.1 are suppressed in the plot. (A color version of this figure can be found in the online supplementary material.)

grids, the maximum solution value becomes even larger). With the saturating form of function g, the onset of aggregation becomes visible only much later than with the other two forms. This can be understood from observing that at the low initial cell densities ($\approx$0.1), the saturating form gives $g \sim \alpha u/2$, whereas $g \sim \alpha u$ for the other two functional forms; the adhesive pull driving aggregation is therefore much lower. Once the clusters have formed, a slow but steady increase in the maximum density occurs, which only flattens off as the density increases above 10 and the impact of the saturation in g takes hold. Finally, the logistic form for function g leads, like the linear form, to a quick formation of cell aggregates. However, unlike in the linear case, the maximum cell density is much smaller here and appears to be bounded by $\approx$4. This value is larger than the parameter $U_{max} = 2$; for the dependence of the maximum cell density on the value of α, see Figure 12.3 (right). In a reduction of

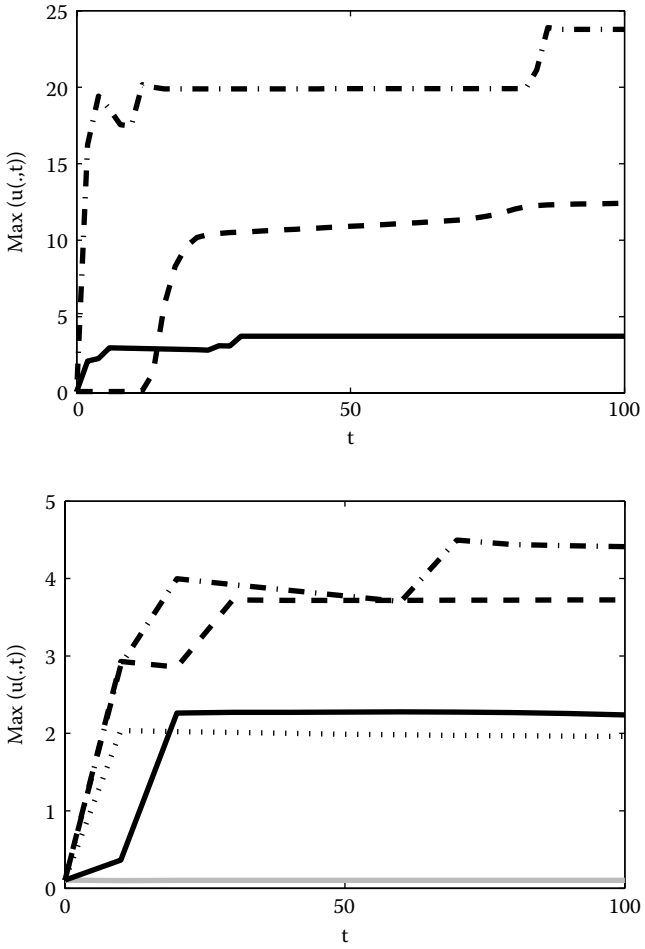

Figure 12.3 (Left) The maximum cell density as a function of time for the numerical experiments shown in Figure 12.2 using $\alpha = 30$ and a function g that is of linear (dot-dashed), saturating (dashed), or logistic (solid) type. (Right) The maximum cell density as a function of time for the numerical experiment shown in Figure 12.2 (bottom), i.e., with logistic type function g, but with different α values: no aggregation for $\alpha = 12$ (solid gray line) and aggregation for $\alpha = 16$ (solid), $\alpha = 20$ (dotted), $\alpha = 30$ (dashed), and $\alpha = 40$ (dot-dashed).

the 2-D case to a quasi-1-D problem, Sherratt et al. [64] have shown that the density is bounded by $U_{max} = 2$, provided the adhesion parameter α is below some critical value; consequently, this result appears either not to generalize to the genuinely 2-D setting or imposes additional constraints on the size of α for boundedness by U_{max}.

Based on the reasonably fast aggregation and the capacity to bound cell densities at lower levels, the choice of the logistic form for function g is recommended and will be considered in the remainder of this chapter.

12.4 Modeling Cell-Cell Sorting

In this section we aim to demonstrate whether the continuous framework developed in Section 12.3 can replicate the predictions of the DAH for cell sorting; cf. Figure 12.1. The prototypical setting here is to consider two cell populations that differ only in their adhesive properties. Initially, the two cell populations are distributed more or less arbitrarily and one is interested in the long-term configuration of the system; see Figure 12.1. We denote the densities of the two cell populations by $u_A(\mathbf{x}, t)$ and $u_B(\mathbf{x}, t)$. It is reasonable to assume that cell proliferation is negligible on the time scale of cell sorting and we further assume that the random motility coefficient is approximately the same for each population. Under these simplifications we obtain the following set of PDEs describing the spatio-temporal evolution of the system:

$$\frac{\partial u_i(\mathbf{x}, t)}{\partial t} = D\nabla^2 u_i - \nabla \cdot \left[\frac{\phi u_i}{R} \int_V \frac{\mathbf{r}}{|\mathbf{r}|} \Omega(|\mathbf{r}|) g_i(u_A(\mathbf{x}+\mathbf{r}, t), u_B(\mathbf{x}+\mathbf{r}, t))\, d\mathbf{r} \right], \quad i = A, B \tag{12.10}$$

This system is considered on the 2-D spatial domain $(0, 10)^2 \subset \mathbb{R}^2$ and complemented with periodic boundary conditions for both species. We consider two sets of initial conditions $u_A(\mathbf{x}, 0)$ and $u_B(\mathbf{x}, 0)$, corresponding to the left- and right-most frames of Figure 12.1a: a single pellet of randomly mixed cell types, Figure 12.4 (center row, left), and a pellet of cell type A juxtaposed to a pellet of cell type B, Figure 12.4 (bottom row, left). The initial masses of cell types A and B are approximately equal for the initial condition shown in Figure 12.4 (center row, left), whereas there is a larger initial mass of cell type B in Figure 12.4 (bottom row, left).

The functions g_i in the cell adhesion term are parameterized by the self- and cross-adhesion parameters, $S_{AA}, S_{BB}, C_{AB} = S_{AB} = S_{BA}$ of the two cell types and we employ a logistic functional form (cf. Section 12.3.1, [6,64]):

$$g_i(u_A, u_B) := (S_{iA}u_A + S_{iB}u_B) \max\left\{0, 1 - \frac{u_A + u_B}{U_{max}}\right\}, \quad i = A, B \tag{12.11}$$

The contributions $S_{ii}u_i$ account for self-adhesion whereas $S_{ij}u_j$ with $i \neq j$ account for cross-adhesion. The factor $\max\{0, 1 - \frac{u_A+u_B}{U_{max}}\}$ is employed to limit the density to which an aggregate can reach; see the effect of the various forms for g in Figure 12.2. Under this form, the adhesive pull of a region increases at lower cell densities before decreasing at higher densities. The sensing region V is a circle with radius one and we use

$$D = \phi = R = 1, \quad \Omega(|\mathbf{r}|) = 1 \text{ for } |\mathbf{r}| \in [0, 1], \quad U_{max} = 1 \tag{12.12}$$

Our first test is to demonstrate the capacity of Equation (12.10) to predict various final configurations according to the self- and cross-adhesion parameters, as illustrated in Figure 12.1. Accordingly, we start with a random mixture of cells of the

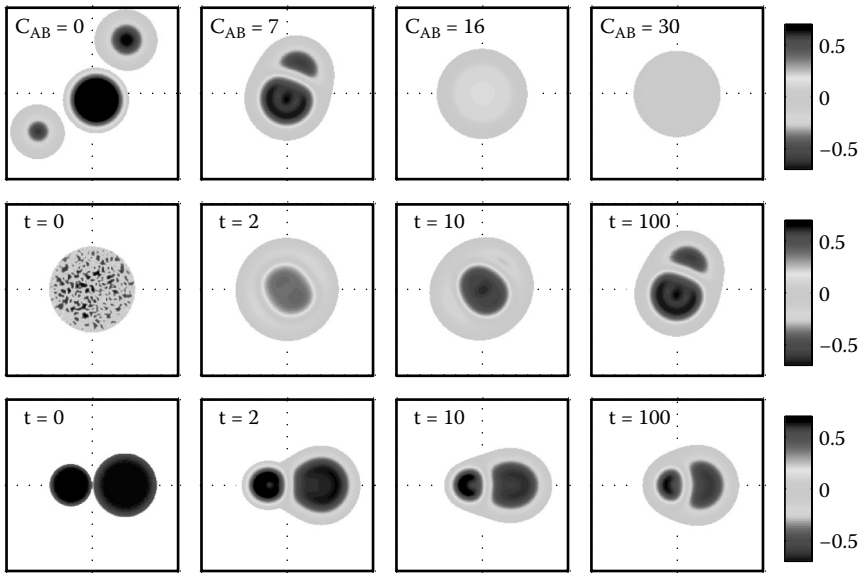

Figure 12.4 The plots show numerical approximations to the cell density differences $u_A(\mathbf{x}, t) - u_B(\mathbf{x}, t)$ of the cell-cell sorting model (Equation (12.10)). In regions with cell densities $u_A < 0.05$ and $u_B < 0.05$, the difference value is suppressed in the plots. (Top Row) The difference is plotted at time $t = 100$, when a (numerical) steady state is reached, for four different values of the cross-adhesion parameter C_{AB} and starting with the initial condition consisting of a single pellet with randomly mixed cell types (described below); all other parameters are as detailed in the main text. Depending on the choice of C_{AB}, from left to right, the four final configurations "complete sorting," "partial engulfment," "engulfment," and "mixing," cf. Figure 12.1c, are attained. (Middle and Bottom Rows) The plots show the time courses as solutions evolve to the steady-state distribution for the fixed cross-adhesion parameter $C_{AB} = 7$ but for the two different initial cell distributions; all other parameters are as detailed in the main text. For the middle row we initially consider a single pellet of radius 2.5 in the center of the domain with a random mixture of cells of type A and B such that $u_A(\mathbf{x}, 0) + u_B(\mathbf{x}, 0) = 0.8$ in the pellet's center and slightly decreasing toward the periphery; densities are zero outside the pellet. For the bottom row we initially consider two adjacent cell pellets, of radii 1.25 (type A) and $\approx$1.87 (type B), containing one cell type each at a density of $\approx$0.8; densities are zero outside the pellets. (This figure together with movies can be found in the online supplementary material.)

two types in a pellet centered in the domain. The self-adhesion coefficients are fixed at $S_{AA} = 30$ and $S_{BB} = 15$ (i.e., population A has stronger self-adhesion), and we consider the impact of variation in the cross-adhesion strength C_{AB}. The results of the simulations are represented by plotting the differences of the cell densities u_A and u_B at large times (i.e., at numerical steady states), shown in Figure 12.4 (top row). Depending on the value of C_{AB}, the steady-state distribution attained corresponds

to that predicted by the DAH based on the relative size of the adhesion coefficients (cf. Figure 12.1c. In particular, it is noted that the more strongly adhesive cell type A tends to accumulate in the center of the pellet, except for the case without any cross-adhesion, $C_{AB} = 0$, that is, total separation.

As a second exploration, we investigate the relatively insensitive nature of the final configuration with respect to the initial distribution of the populations (cf. Figure 12.1a). Here we choose $S_{AA} = 30$, $S_{BB} = 15$, and $C_{AB} = 7$; according to the DAH this predicts the partial engulfment of A by B at the steady state. Starting from the two sets of initial conditions described above, the time courses as solutions evolve to the steady-state distribution are plotted in the middle and bottom rows of Figure 12.4. Clearly, we observe evolution to the same pattern phenotype at the steady state; the differences in the right-most configurations stem from the smaller proportion of A used in the bottom row.

As a final test of the continuous cell sorting model, we explore whether Equation (12.10), when extended to three cell populations, can predict the hierarchical relationship of adhesive populations, similar to Figure 12.1b. For three populations A, B, and C obeying the self-adhesion hierarchy $S_{AA} > S_{BB} > S_{CC}$, simulations predict that population A becomes engulfed at the center, population C is confined to the periphery, and population B is sandwiched between A and C; Figure 12.5.

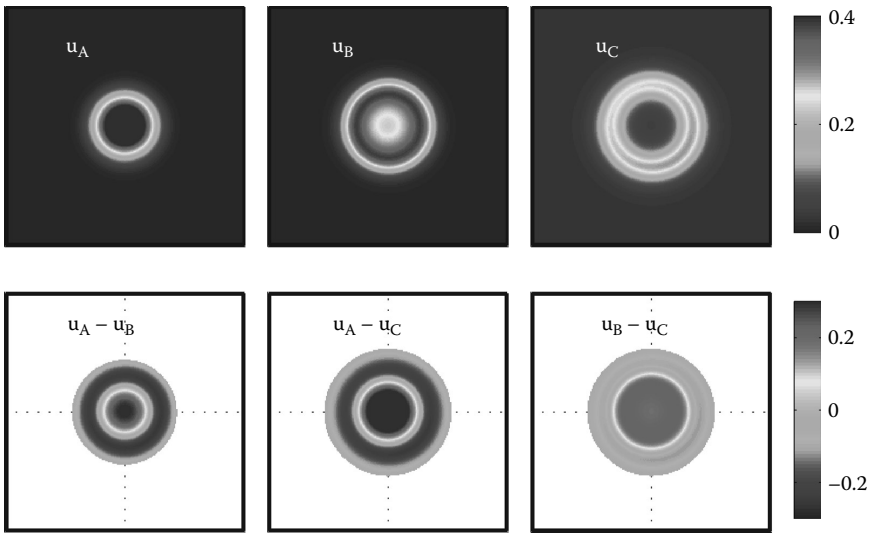

Figure 12.5 The plots show numerical solutions of Equation. (12.10) extended to three cell types A, B, and C. (Top Row) Solutions u_A, u_B, and u_C at time $t = 50$. (Bottom Row) Pairwise solution differences at time $t = 50$. The initial condition is a randomly mixed pellet of the three cell types. The adhesion parameters are $S_{AA} = 45$, $S_{BB} = 30$, $S_{CC} = 15$, $C_{AB} = 31$, $C_{AC} = 0$, $C_{BC} = 16$. (This figure together with a movie can be found in the online supplementary material.)

12.5 Modeling Adhesion during Cancer Invasion

In this section we demonstrate the applicability of the continuous framework for cellular adhesion by considering a simple and minimalist model of cancer cell invasion into healthy tissue, (cf. [33]). The model consists of three equations describing the cancer cell density (c), the extracellular matrix (ECM) density (v), and the concentration of a (generic) matrix degrading enzyme (MDE) (m). The model equations are given by:

$$\frac{\partial c(\mathbf{x}, t)}{\partial t} = D_1 \nabla^2 c - \nabla \cdot \left[\frac{\phi c}{R} \int_V \frac{\mathbf{r}}{|\mathbf{r}|} \Omega(|\mathbf{r}|) g(c(\mathbf{x}+\mathbf{r}, t), v(\mathbf{x}+\mathbf{r}, t))\, d\mathbf{r} \right] + \mu_1 c(1 - c - v) \tag{12.13a}$$

$$\frac{\partial v(\mathbf{x}, t)}{\partial t} = -\gamma m v + \mu_2 (1 - c - v) \tag{12.13b}$$

$$\frac{\partial m(\mathbf{x}, t)}{\partial t} = D_3 \nabla^2 m + \alpha c - \lambda m \tag{12.13c}$$

For simplicity, we restrict our attention to a 2-D geometry and consider the above equations on the spatial domain $(-1.5, 1.5)^2 \subset \mathbb{R}^2$, subject to periodic boundary conditions. In this model, both the cancer cells and ECM occupy physical space while the volume occupied by MDE is assumed negligible. The cancer and ECM density equations above have been normalized such that the total density $c + v = 1$ characterizes fully occupied physical space.

In this simple model, cancer cell migration is assumed to arise from (1) random motility (the corresponding coefficient D_1 is rather small) and (2) a directed movement due to adhesive effects of cancer cells with themselves and the surrounding ECM. The sensing region V for the adhesion term is a circle of radius $R = 0.1$ and for the function $\Omega(|\mathbf{r}|)$ we select a linearly decaying function

$$\Omega(|\mathbf{r}|) = \frac{3}{\pi R^2} \left(1 - \frac{|\mathbf{r}|}{R} \right) \quad \text{for} \quad |\mathbf{r}| \in [0, R] \tag{12.14}$$

The linear decay of $\Omega(|\mathbf{r}|)$ models a diminishing influence of adhesive bonds toward the periphery of the sensing region. The leading factor in $\Omega(|\mathbf{r}|)$ follows from a normalization ensuring that the integral of $\Omega(|\mathbf{r}|)$ over the sensing region V is equal to one, stipulating a fixed maximum capacity of cells to form adhesive bonds within the sensing region independent of its actual size. The magnitude of that capacity is captured in the (parameters of the) function g, which takes the form

$$g(c, v) = (S_{cc} c + S_{cv} v) \max\{0, 1 - (c + v)\} \tag{12.15}$$

This functional form implies that cancer cells adhere to themselves (self-adhesion parameter S_{cc}) and to the matrix (cross-adhesion parameter S_{cv}). Again, we include the limiting term such that g becomes zero if the total density $c + v$ approaches the

value one. In addition to cell migration, cancer cell proliferation is also incorporated through the employment of a logistic growth type law with growth rate μ_1 and "carrying capacity" dependent on the locally available space, $1 - c - v$.

The ECM is assumed to be nonmotile and degraded upon contact by MDEs at a rate γ. In the general formulation, a simple ECM production term permits regeneration of the ECM with rate μ_2 (note that in the simulations below, it is assumed that $\mu_2 = 0$). Finally, MDEs diffuse throughout the tissue (with diffusion constant D_3), are produced by the cells at rate α, and decay at rate λ. The following set of parameters is used in the simulation

$$\begin{array}{lllll} D_1 = 10^{-3}, & D_3 = 10^{-3}, & \mu_1 = 0.1, & \mu_2 = 0, & \alpha = 0.1, \\ \gamma = 10, & \lambda = 0.5, & R = 0.1, & S_{cc} = 0.05, & S_{cv} = 0.1 \end{array} \tag{12.16}$$

Clearly, the model in Equations (12.13) through (12.16) is highly simplified in its nature and excludes many pertinent biochemical interactions. However, the focus here is on the incorporation and effect of the adhesion term in a model of tumor invasion and, consequently, we wish to retain the simplicity of the model. Crucial questions for any model of cancer invasion are whether it permits the breakage of cancer cells from a central tumor mass and how cancer cell migration is affected by a heterogeneous tumor environment. To address these issues, we consider an initial tumor population concentrated at the center of the domain (representing the central tumor mass) and lying within a spatially structured ECM matrix. The initial MDE concentration is chosen to be proportional to the cell density. Simulations for a striped distribution in the initial ECM densities are shown in Figures 12.6 and 12.7.

In Figure 12.6 we observe the preferential accumulation and invasion of cancer cells along stripes of higher ECM density, in concert with degradation of that ECM. Cell migration obeys the restriction of physical space, that is, cells do not move into densely packed tissue. Cells at the tumor periphery do not accumulate in regions of low ECM density, but rather quickly cross these areas to concentrate at the front of the next ECM barrier. The variation in ECM density also leads to the formation of protrusions that stretch from the cancer mass into the healthy tissue. Due to the regular structure of the ECM, these protrusions are also regular. Similar results apply when cell proliferation is excluded; however, the protrusions now take the form of high-density tumor clumps extending along the ECM stripes; Figure 12.7.

12.6 Discussion and Outstanding Questions

In this chapter we discussed the critical role played by cellular adhesion during a wide spectrum of biological processes, highlighting the need for mathematical models to capture this fundamental phenomenon. A brief review of existing models, discrete and continuous, has demonstrated their individual strengths and weaknesses. Of particular note is the lack of continuous models that can replicate the "sorting" behavior

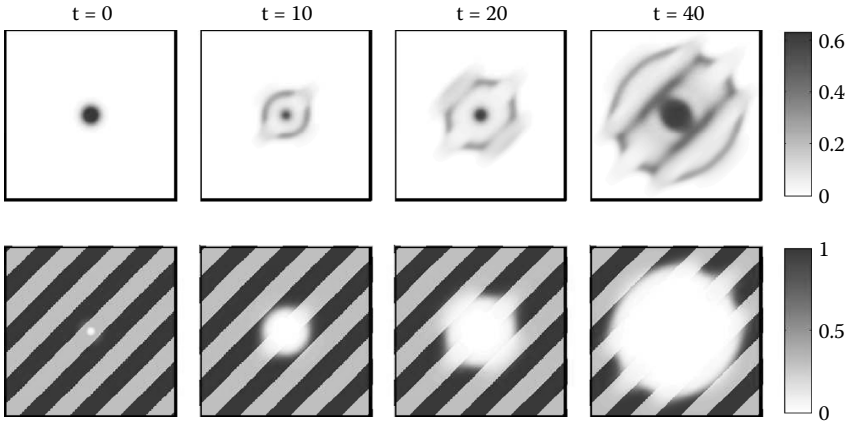

Figure 12.6 Simulation results for model in Equation (12.13) through (12.16) with a diagonally striped initial ECM distribution. Shown are the tumor cell density (top row) and the ECM density (bottom row) in the central part $(-1, 1)^2$ of the spatial domain at four time points. The MDE concentration displays similar features as the cell density and is not shown. (A color version of this figure together with a movie can be found in the online supplementary material.)

of multiple adhesive populations. As far as we are aware, the only continuous model that has been demonstrated to capture this property is that developed in [6]. Here we expanded the derivation of this model and corroborated its suitability through an extended numerical analysis that replicates the wide variety of cell sorting "experiments," as predicted by the Differential Adhesion Hypothesis (DAH). The ultimate

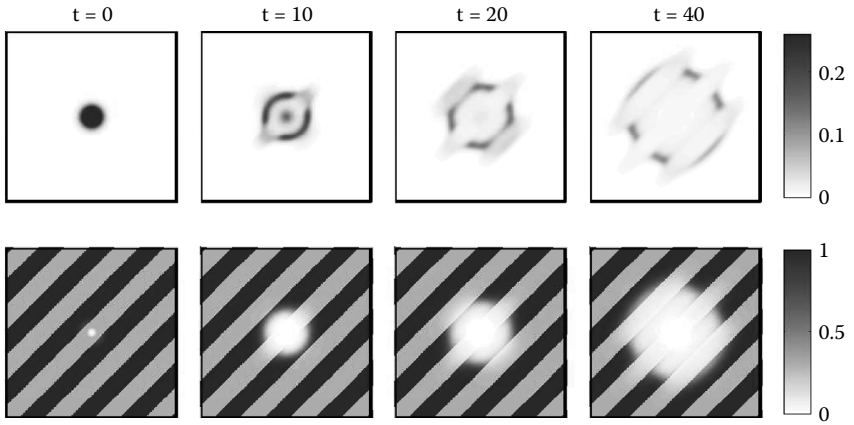

Figure 12.7 Simulation results for model in Equations (12.13) through (12.16) as in Figure 12.6 but without cancer cell proliferation (i.e., $\mu_1 = 0$). (A color version of this figure together with a movie can be found in the online supplementary material.)

success of this approach lies in its capacity for integration with existing continuous models; as a demonstration of its suitability, we considered its extension into a model for cancer invasion as originally studied in [33] (see also [64]). A second application, considered in [7], has been to the process of chick somitogenesis. There it was shown that upregulation of cellular adhesion, regulated through an underlying chemical signaling network, could drive both the epithelialization and subsequent sorting of pre-somitic cells into somites. The ubiquity of cellular adhesion would allow a catalog of potential applications to be listed: some typical examples, based on the history of modeling in these areas, include angiogenesis, wound healing, development of the slime mold *Dictyostelium*, and skeletal patterning.

In the continuous adhesion model, the microscopic processes (e.g., receptor binding) can be accounted for by a suitable choice of cell adhesion parameters. A crucial extension of this work lies in the development of truly multiscale models of cell adhesion, in which the sizes of adhesion parameters in the continuous model can be determined from the processes occurring at a microscopic scale. To achieve this, it will be necessary to derive models for cell adhesion from a realistic underlying description of individual cell behavior; as discussed in Section 12.2, a number of attempts have been made at exploring some of these issues (e.g., see [52,76]).

Mathematically, a striking feature in the modeling approach is that cellular adhesion is accounted for via a nonlocal (integral) advective type term. As such, this fits coherently into the typical taxis-diffusion-reaction frameworks frequently employed in the modeling of pattern-formation type phenomena. Similarly, existing simulation packages for diffusion-reaction systems can be extended in modular fashion to allow the incorporation of such nonlocal terms. One difficulty, however, is the additional computational effort required to evaluate the nonlocal term. A suitable solution to this problem is outlined in the Appendix to this chapter, the scheme in which provides high-resolution simulations within reasonable computing times (at least for the case of a rectangular spatial domain with periodic boundary conditions). However, extra work will be required to extend the numerical techniques to more general situations, such as irregular geometries or three dimensions.

Analytically, a number of results are available on the properties of solutions. In [64], the boundedness of solutions was addressed under particular forms of the model. Specifically, it was shown (in one dimension) that for $g(u) = \alpha u \max\{0, 2-u\}$, boundedness of u below 2 is possible under specific restrictions for the size of α and form of $\Omega(|\mathbf{r}|)$. In [38] a related nonlocal model for chemotaxis was derived and global existence of solutions was proven for all finite sampling radii. A considerable number of questions, however, remain unanswered. Of particular interest are an extension of the boundedness results to spatially 2-D settings, the proper incorporation of other boundary conditions from both an analytical as well as a modeling point of view, and an analysis of the limiting scenario as the sampling radius $R \to 0$.

The formulation of the model presented here clearly simplifies many crucial components regarding the behavior of adhesive populations *in vivo*. For example, the dynamics of adhesive binding are assumed to correlate to overall cell/matrix densities rather than the concentrations of adhesive molecules at the cell membrane, the dynamics of which can vary both spatially and temporally according to intra- and

extracellular signals. Further, while adhesion is assumed here only to generate forces resulting in cell migration, the signaling initiated through binding interplays with many facets of cell behavior, including division and apoptosis. Extending the model to include some of these complexities will further advance its relevance to understanding the role of adhesion in a wide variety of biological processes.

12.7 Appendix: Numerical Method

The models in this chapter are all solved following the Method of Lines (MOL). The rectangular spatial domain is covered with a uniform grid where each grid cell, or finite volume, is a square of side length h. In a first step of the MOL, the spatial derivatives are discretized on that grid and we employ a Finite Volume Method (FVM) of order 2 (see, e.g., [32]). This transforms the PDE model into a large and, in general, stiff system of ordinary differential equations (ODEs), the MOL-ODE system:

$$\frac{\mathrm{d}\mathbf{U}(\mathrm{t})}{\mathrm{dt}} = \mathcal{F}(\mathrm{t}, \mathbf{U}(\mathrm{t}))\,, \quad \mathbf{U}(0) = \mathbf{U_0} \tag{12.17}$$

As is customary when using the FVM, the components of this ODE system represent approximations to the averages of the PDE solution in each finite volume. The numerical solution of the MOL-ODE in Equation (12.17) constitutes the second step of the MOL and an appropriate time integration scheme must be selected. Implicit time integration schemes can deal efficiently with the inherent stiffness of the MOL-ODE. We favor the linearly implicit, fourth-order Runge-Kutta method ROWMAP [78]. The multiple Arnoldi process used within this method for the solution of the linear equation systems in each time step makes this scheme particularly suited for the large ODE system at hand. Furthermore, the method does not require any computation of the Jacobian of the MOL-ODE by the user; the required Jacobian-times-vector products are computed automatically by a suitable finite difference approximation using the right-hand-side $\mathcal{F}$ of the MOL-ODE.

The FVM described in [32] has been applied to taxis-diffusion-reaction systems. There, difficulties arise in regions of strong variation of the solution of the PDE, for example, near moving fronts. These are due to the taxis term of the model and special attention was given to ensure that the discretization of that term does not introduce oscillations or negative solution values in the solution of the MOL-ODE. This goal can be achieved, while maintaining the order two of the FVM as much as possible, using a second-order upwind discretization together with a nonlinear limiter function. The models of this chapter have a nonlocal adhesion term that is similar to the taxis terms in [32]. So we apply the same discretization to that term, with the added difficulty of the approximation of the integral. The adhesion term, in general, takes the following

form for the adhesive species u_i of a vector $\mathbf{u}$ of concentrations or densities in the models

$$-\nabla \cdot [u_i(\mathbf{x}, t) \underbrace{\frac{\phi}{R} \int_V \frac{\mathbf{r}}{|\mathbf{r}|} \Omega(|\mathbf{r}|) g_i(\mathbf{u}(\mathbf{x}+\mathbf{r}, t))\, d\mathbf{r}}_{\text{the adhesive velocity in } (\mathbf{x}, t)}] \tag{12.18}$$

The adhesive velocity, and consequently the integral, must be approximated on each edge of the spatial grid for each evaluation of the right-hand side of the MOL-ODE. This task constitutes the computational bottleneck of the whole numerical solution process. If we assume that (1) the sensing region V at each $\mathbf{x}$ is the same and time independent, and (2) that we solve the PDE system on a rectangular domain with periodic boundary conditions, then the adhesive velocity in Equation (12.18) can be approximated on all vertical (or all horizontal) edges of the spatial grid simultaneously by evaluating a matrix-vector product $M\mathbf{G}$. Here, the matrix $M \in \mathbb{R}^{N,N}$, N the number of grid cells, and each row of M corresponds to the approximation of the nonlocal term on one edge. We arrive at this by first evaluating function g_i at the approximation $\mathbf{U}(t)$ yielding $\mathbf{G} \in \mathbb{R}^N$; second by reconstructing a function $\tilde{g}_i(\mathbf{x})$ from that data using bilinear interpolation; and third, by approximating the integral with $\tilde{g}_i$ instead of g_i. Thanks to a suitable basis representation of $\tilde{g}_i$, the matrix M will be independent of the data $\mathbf{G}$ and can be precomputed before the time integration of Equation (12.17) commences. Furthermore, the third step can be performed to any desired accuracy so that the overall accuracy of the nonlocal term evaluation hinges solely on the quality of the reconstruction of function g_i by $\tilde{g}_i$, that is, can be controlled by the spatial grid width h. Typically, the sensing region V is much smaller than the spatial domain of the PDE model. Consequently, the matrix M contains many zeros. However, in contrast to the approximation of derivatives, the fraction of non-zero elements of M remains constant with decreasing spatial grid width h. In that sense, sparse matrix techniques can only have a limited impact for the efficient evaluation of the matrix-vector product $M\mathbf{G}$. At this point the periodic boundary conditions become important. These give rise to a matrix M having the structure of a block-circulant matrix with circulant blocks. Matrix-vector products with such matrices can be evaluated efficiently with Fast Fourier Transform (FFT) techniques. This substantially reduces the computational complexity and hence CPU time requirements for the evaluation of $M\mathbf{G}$. More details of the integral approximation and evaluation can be found in [31].

In the discussion above we have assumed periodic boundary conditions for the PDE problem. This is not always suitable from the point of view of modeling. No-flux boundary conditions are frequently encountered and in the following we describe how they can be included in the computational framework. For the nonlocal term, the boundary conditions become only important in points $\mathbf{x}$ where the set V, centerd at $\mathbf{x}$, intersects the boundary of the spatial domain of the PDE. For such $\mathbf{x}$ we follow the approach taken in [7]: that the integral of the nonlocal term is taken only over those $\mathbf{r} \in V$ such that $\mathbf{x} + \mathbf{r}$ is within the spatial domain. This modification implies that the matrix M changes from a block-circulant matrix with circulant blocks to a block-Toeplitz matrix with Toeplitz blocks. FFT techniques cannot be applied directly to such matrices but any such matrix can be embedded into a block-circulant matrix

$\tilde{\mathrm{M}}$ with circulant blocks. The size of $\tilde{\mathrm{M}}$ will be larger than the size of M but for our application the increase will be modest. The vector $\mathbf{G}$ must also be padded with zeros in appropriate places to yield the extended vector $\tilde{\mathbf{G}}$. Now, the result vector of the matrix-vector product $\mathrm{M}\mathbf{G}$, which we want to compute, can be extracted from the result vector of the efficiently to evaluate the extended matrix-vector product $\tilde{\mathrm{M}}\tilde{\mathbf{G}}$. We illustrate this for the Toeplitz to circulant case (i.e., no block structure), which is applicable for the simulation of spatially 1-D models. In that case, the matrix M is a banded Toeplitz matrix with, say, upper bandwidth m and lower bandwidth n

$$\mathrm{M} = \begin{pmatrix} \mathrm{l}_0 & \mathrm{l}_1 & \dots & \mathrm{l}_\mathrm{m} & 0 & \dots & 0 \\ \mathrm{l}_{-1} & \ddots & \ddots & & \ddots & \ddots & \\ \vdots & \ddots & & & & & \\ \mathrm{l}_{-\mathrm{n}} & & & & & & \\ 0 & \ddots & & & & & \\ \vdots & \ddots & & & & & \\ 0 & & & & & & \end{pmatrix} \in \mathbb{R}^{\mathrm{N},\mathrm{N}} \tag{12.19}$$

The corresponding circulant matrix $\tilde{\mathrm{M}}$ then has $\mathrm{N} + \max\{\mathrm{n}, \mathrm{m}\}$ rows and columns and is defined by its first column

$$(\mathrm{l}_0, \mathrm{l}_{-1}, \dots, \mathrm{l}_{-\mathrm{n}}, 0 \dots, \mathrm{l}_\mathrm{m}, \mathrm{l}_{\mathrm{m}-1}, \dots, \mathrm{l}_1)^\mathsf{T} \in \mathbb{R}^{\mathrm{N}+\max\{\mathrm{n},\mathrm{m}\}} \tag{12.20}$$

The extended vector $\tilde{\mathbf{G}}$ is given by $\tilde{\mathbf{G}} = (\mathbf{G}, \mathbf{0})^\mathsf{T} \in \mathbb{R}^{\mathrm{N}+\max\{\mathrm{n},\mathrm{m}\}}$ and then holds

$$\mathrm{M}\mathbf{G} = \left[\tilde{\mathrm{M}}\tilde{\mathbf{G}}\right]_{1,\dots,\mathrm{N}} \tag{12.21}$$

That is, only the first N entries of $\tilde{\mathrm{M}}\tilde{\mathbf{G}}$ are used.

References

[1] B. Alberts, A. Johnson, J. Lewis, M. Raff, K. Roberts, and P. Walter (2002). *Molecular Biology of the Cell*, 4th edition. Garland Science, Taylor & Francis Group.

[2] A.R.A. Anderson (2005). A hybrid mathematical model of solid tumour invasion: the importance of cell adhesion. *IMA J. Math. Med. Biol.* 22:163–186.

[3] A.R.A. Anderson, M.A.J. Chaplain, E.L. Newman, R.J.C. Steele, and A.M. Thompson (2000). Mathematical modelling of tumour invasion and metastasis. *Comput. Math. Meth. Med. (*formerly *J. Theor. Med.)* 2:129–154.

[4] A.R.A. Anderson, A.M. Weaver, P.T. Cummings, and V. Quaranta (2006). Tumor morphology and phenotypic evolution driven by selective pressure from the microenvironment. *Cell* 127:905–915.

[5] K. Anguige and C. Schmeiser (2009). A one-dimensional model of cell diffusion and aggregation, incorporating volume filling and cell-to-cell adhesion. *J. Math. Biol.* 58(3):395–427.

[6] N.J. Armstrong, K.J. Painter, and J.A. Sherratt (2006). A continuum approach to modelling cell-cell adhesion. *J. Theor. Biol.* 243:98–113.

[7] N.J. Armstrong, K.J. Painter, and J.A. Sherratt (2009). Adding adhesion to a chemical signaling model for somite formation. *Bull. Math. Biol.* 71:1–24.

[8] K.M. Bagnall, S.J. Higgins, and E.J. Sanders (1989). The contribution made by cells from a single somite to tissues within a body segment and assessment of their integration with similar cells from adjacent segments. *Development* 107:931–943.

[9] A.L. Bauer, T.L. Jackson, and Y. Jiang (2007). A cell-based model exhibiting branching and anastomosis during tumor-induced angiogenesis. *Biophys. J.* 92:3105–3121.

[10] A.L. Berrier and K.M. Yamada (2007). Cell-matrix adhesion. *J. Cell. Physiol.* 213:565–573.

[11] W. Birchmeier (1994). Molecular aspects of the loss of cell adhesion and gain of invasiveness in carcinomas. *Int. Symp. Princess Takamatsu Cancer Res. Fund* 24:214–232.

[12] H.M. Byrne and M.A.J. Chaplain (1996). Modelling the role of cell-cell adhesion in the growth and development of carcinomas. *Math. Comput. Modelling* 24:1–17.

[13] R.W. Carthew (2007). Pattern formation in the *Drosophila* eye. *Curr. Opin. Genet. Dev.* 17:309–313.

[14] U. Cavallaro and G. Christofori (2004). Cell adhesion and signalling by cadherins and Ig-CAMs in cancer. *Nat. Rev. Cancer* 4:118–132.

[15] U. Cavallaro and G. Christofori (2004). Multitasking in tumor progression: signaling functions of cell adhesion molecules. *Ann. N.Y. Acad. Sci.* 1014:58–66.

[16] C.M. Cheney and J.W. Lash (1984). An increase in cell-cell adhesion in the chick segmental plate results in a meristic pattern. *J. Embryol. Exp. Morphol.* 79:1–10.

[17] G. Christofori (2003). Changing neighbours, changing behaviour: cell adhesion molecule-mediated signalling during tumour progression. *EMBO J.* 22:2318–2323.

[18] V. Cristini, J. Lowengrub, and Q. Nie (2003). Nonlinear simulation of tumor growth. *J. Math. Biol.* 46:191–224.

[19] J.C. Dallon and H.G. Othmer (2004). How cellular movement determines the collective force generated by the Dictyostelium discoideum slug. *J. Theor. Biol.* 231:203–222.

[20] A. Deutsch (1999). Cellular Automata and Biological Pattern Formation. Habilitation thesis, University of Bonn.

[21] A. Deutsch and S. Dormann (2005). *Cellular Automaton Modeling of Biological Pattern Formation: Characterization, Applications, and Analysis*. Boston, Birkhäuser.

[22] R. Dillon, K.J. Painter, and M.R. Owen (2008). A single-cell based model of cellular growth using the immersed boundary method. In B. Cheong Koo, Z. Li, and P. Li, Eds., *Moving Interface Problems and Applications in Fluid Dynamics*, Contemporary Mathematics. AMS, 1–16.

[23] D. Drasdo, R. Kree, and J.S. McCaskill (1995). Monte Carlo approach to tissue-cell populations. *Phys. Rev. E* 52:6635–6657.

[24] J.L. Duband, S. Dufour, K. Hatta, M. Takeichi, G.M. Edelman, and J.P. Thiery (1987). Adhesion molecules during somitogenesis in the avian embryo. *J. Cell. Biol.* 104:1361–1374.

[25] D. Duguay, R.A. Foty, and M.S. Steinberg (2003). Cadherin-mediated cell adhesion and tissue segregation: qualitative and quantitative determinants. *Dev. Biol.* 253:309–323.

[26] G.A. Dunn and J.P. Heath (1976). A new hypothesis of contact guidance in tissue cells. *Exp. Cell Res.* 101:1–14.

[27] R.A. Foty and M.S. Steinberg (2004). Cadherin-mediated cell-cell adhesion and tissue segregation in relation to malignancy. *Int. J. Dev. Biol.* 48:397–409.

[28] R.A. Foty and M.S. Steinberg (2005). The differential adhesion hypothesis: a direct evaluation. *Dev. Biol.* 278:255–263.

[29] P. Friedl and K. Wolf (2003). Tumour-cell invasion and migration: diversity and escape mechanisms. *Nat. Rev. Cancer* 3:362–374.

[30] J. Galle, G. Aust, G. Schaller, T. Beyer, and D. Drasdo (2006). Individual cell-based models of the spatial-temporal organization of multicellular systems—Achievements and limitations. *Cytometry Part A* 69A:704–710.

[31] A. Gerisch (2008). On the approximation and efficient evaluation of integral terms in PDE models of cell adhesion. *Submitted for publication*.

[32] A. Gerisch and M.A.J. Chaplain (2006). Robust numerical methods for taxis–diffusion–reaction systems: applications to biomedical problems. *Math. Comput. Modelling* 43:49–75.

[33] A. Gerisch and M.A.J. Chaplain (2008). Mathematical modelling of cancer cell invasion of tissue: local and non-local models and the effect of adhesion. *J. Theor. Biol.* 250:684–704.

[34] J.A. Glazier and F. Graner (1993). Simulation of the differential adhesion driven rearrangement of biological cells. *Phys. Rev. E* 47:2128–2154.

[35] F. Graner and J.A. Glazier (1992). Simulation of biological cell sorting using a two-dimensional extended Potts model. *Phys. Rev. Lett.* 69:2013–2016.

[36] B.M. Gumbiner (2005). Regulation of cadherin-mediated adhesion in morphogenesis. *Nat. Rev. Mol. Cell Biol.* 6:622–634.

[37] T. Hillen (2002). Hyperbolic models for chemosensitive movement. *Math. Mod. Meth. Appl. Sci.* 12:1007–1034.

[38] T. Hillen, K. Painter, and C. Schmeiser (2007). Global existence for chemotaxis with finite sampling radius. *Disc. Cont. Dyn. Syst. B (DCDS-B)* 7:125–144.

[39] T. Hillen and K.J. Painter (2009). A user's guide to PDE models for chemotaxis. *J. Math. Biol.* 58:183–217.

[40] G.S. Hillis and A.D. Flapan (1998). Cell adhesion molecules in cardiovascular disease: a clinical perspective. *Heart* 79:429–431.

[41] T. Hofer, J.A. Sherratt, and P.K. Maini (1995). *Dictyostelium discoideum:* cellular self-organization in an excitable biological medium. *Proc. Biol. Sci.* 259:249–257.

[42] K. Horikawa, G. Radice, M. Takeichi, and O. Chisaka (1999). Adhesive subdivisions intrinsic to the epithelial somites. *Dev. Biol.* 215:182–189.

[43] E.F. Keller and L.A. Segel (1970). Initiation of slime mold aggregation viewed as an instability. *J. Theor. Biol.* 26:399–415.

[44] R. Keller (2002). Shaping the vertebrate body plan by polarized embryonic cell movements. *Science* 298:1950–1954.

[45] K.K. Linask, C. Ludwig, M.D. Han, X. Liu, G.L. Radice, and K.A. Knudsen (1998). N-cadherin/catenin-mediated morphoregulation of somite formation. *Dev. Biol.* 202:85–102.

[46] C.M. Lo, H.B. Wang, M. Dembo, and Y.L. Wang (2000). Cell movement is guided by the rigidity of the substrate. *Biophys. J.* 79:144–152.

[47] P. Macklin and J. Lowengrub (2007). Nonlinear simulation of the effect of microenvironment on tumor growth. *J. Theor. Biol.* 245:677–704.

[48] A.F. Marée and P. Hogeweg (2001). How amoeboids self-organize into a fruiting body: multicellular coordination in *Dictyostelium discoideum*. *Proc. Natl. Acad. Sci. USA* 98:3879–3883.

[49] M. Mareel and A. Leroy (2003). Clinical, cellular, and molecular aspects of cancer invasion. *Physiol. Rev.* 83:337–376.

[50] J. Moreira and A. Deutsch (2005). Pigment pattern formation in zebrafish during late larval stages: a model based on local interactions. *Dev. Dyn.* 232:33–42.

[51] T.J. Newman (2005). Modeling multicellular systems using subcellular elements. *Math. Biosci. Eng.* 2:613–624.

[52] T.J. Newman and R. Grima (2004). Many-body theory of chemotactic cell-cell interactions. *Phys. Rev. E* 70:051916.

[53] D. Ostrovsky, C.M. Cheney, A.W. Seitz, and J.W. Lash (1983). Fibronectin distribution during somitogenesis in the chick embryo. *Cell. Differ.* 13: 217–223.

[54] K.J. Painter, D. Horstmann, and H.G. Othmer (2003). Localization in lattice and continuum models of reinforced random walks. *Appl. Math. Lett.* 16:375–381.

[55] E. Palsson (2008). A 3-D model used to explore how cell adhesion and stiffness affect cell sorting and movement in multicellular systems. *J. Theor. Biol.* 254: 1–13.

[56] E. Palsson and H.G. Othmer (2000). A model for individual and collective cell movement in *Dictyostelium discoideum*. *Proc. Natl. Acad. Sci. USA* 97:10448–10453.

[57] S.D. Patel, C.P. Chen, F. Bahna, B. Honig, and L. Shapiro (2003). Cadherin-mediated cell-cell adhesion: sticking together as a family. *Curr. Opin. Struct. Biol.* 13:690–698.

[58] N.J. Popawski, M. Swat, J.S. Gens, and J.A. Glazier (2007). Adhesion between cells, diffusion of growth factors, and elasticity of the AER produce the paddle shape of the chick limb. *Physica A* 373:521–532.

[59] O. Pourquié (2001). Vertebrate somitogenesis. *Annu. Rev. Cell. Dev. Biol.* 17:311–350.

[60] I. Ramis-Conde, D. Drasdo, A.R.A. Anderson, and M.A.J. Chaplain (2008). Modeling the influence of the E-cadherin-beta-catenin pathway in cancer cell invasion: a multiscale approach. *Biophys. J.* 95:155–165.

[61] K.A. Rejniak (2007). An immersed boundary framework for modelling the growth of individual cells: an application to the early tumour development. *J. Theor. Biol.* 247:186–204.

[62] N.J. Savill and J.A. Sherratt (2003). Control of epidermal stem cell clusters by Notch-mediated lateral induction. *Dev. Biol.* 258:141–153.

[63] G. Schaller and M. Meyer-Hermann (2005). Multicellular tumor spheroid in an off-lattice Voronoi-Delaunay cell model. *Phys. Rev. E* 71:051910.

[64] J.A. Sherratt, S. Gourley, N.A. Armstrong, and K.J. Painter (2009). Boundedness of solutions of a nonlocal reaction-diffusion model for cellular adhesion. *Eur. J. Appl. Math.* 20:123–144.

[65] M.S. Steinberg (1962). Mechanism of tissue reconstruction by dissociated cells. II. Time course of events. *Science* 137:762–763.

[66] M.S. Steinberg (1962). On the mechanism of tissue reconstruction by dissociated cells, I. Population kinetics, differential adhesiveness, and the absence of directed migration. *Proc. Natl. Acad. Sci. USA* 48:1577–1582.

[67] M.S. Steinberg (1962). On the mechanism of tissue reconstruction by dissociated cells. III. Free energy relations and the reorganization of fused, heteronomic tissue fragments. *Proc. Natl. Acad. Sci. USA* 48:1769–1776.

[68] M.S. Steinberg (2007). Differential adhesion in morphogenesis: a modern view. *Curr. Opin. Genet. Dev.* 17:281–286.

[69] M.S. Steinberg and M. Takeichi (1994). Experimental specification of cell sorting, tissue spreading, and specific spatial patterning by quantitative differences in cadherin expression. *Proc. Natl. Acad. Sci. USA* 91:206–209.

[70] C.D. Stern and R.J. Keynes (1987). Interactions between somite cells: the formation and maintenance of segment boundaries in the chick embryo. *Development* 99:261–272.

[71] M. Takeichi (1988). The cadherins: cell-cell adhesion molecules controlling animal morphogenesis. *Development* 102:639–655.

[72] M. Takeichi (1995). Morphogenetic roles of classic cadherins. *Curr. Opin. Cell Biol.* 7:619–627.

[73] U. Tepass, D. Godt, and R. Winklbauer (2002). Cell sorting in animal development: signalling and adhesive mechanisms in the formation of tissue boundaries. *Curr. Opin. Genet. Dev.* 12:572–582.

[74] P.L. Townes and J. Holtfreter (1955). Directed movements and selective adhesion of embryonic amphibian cells. *J. Exp. Zool.* 128:53–120.

[75] S. Turner and J.A. Sherratt (2002). Intercellular adhesion and cancer invasion: a discrete simulation using the extended Potts model. *J. Theor. Biol.* 216:85–100.

[76] S. Turner, J.A. Sherratt, and D. Cameron (2004). Tamoxifen treatment failure in cancer and the nonlinear dynamics of TGFβ. *J. Theor. Biol.* 229:101–111.

[77] S. Turner, J.A. Sherratt, K.J. Painter, and N.J. Savill (2004). From a discrete to a continuous model of biological cell movement. *Phys. Rev. E* 69:021910.

[78] R. Weiner, B.A. Schmitt and H. Podhaisky (1997). ROWMAP—a ROW-code with Krylov techniques for large stiff ODEs. *Appl. Numer. Math.* 25:303–319.

[79] M.J. Wheelock, Y. Shintani, M. Maeda, Y. Fukumoto, and K. Johnson (2008). Cadherin switching. *J. Cell. Sci.* 121:727–735.

[80] S.M. Wise, J.S. Lowengrub, H.B. Frieboes, and V. Cristini (2008). Three-dimensional multispecies nonlinear tumor growth—I: Model and numerical method. *J. Theor. Biol.* 253:524–543.

[81] W. Wood and P. Martin (2002). Structures in focus—filopodia. *Int. J. Biochem. Cell Biol.* 34:726–730.